ADVANCING EARTH AND SPACE SCIENCE

JGR Earth Surface

RESEARCH ARTICLE
10.1029/2018JF004861

Intertidal Creeks and Overmarsh Circulation in a Small Salt Marsh Basin

Jessica Chassereau Sullivan[1], **Raymond Torres**[2], **and Alfred Garrett**[3]

[1]Department of Biology and Geology, University of South Carolina Aiken, Aiken, SC, USA, [2]Department of Earth and Ocean Science, University of South Carolina, Columbia, SC, USA, [3]Savannah River National Laboratory, Savannah River Site, Aiken, SC, USA

Key Points:
- First- and second-order creeks play a minor role in overmarsh circulation
- Higher-order creeks are associated with short-circuiting conduits and greatly impact overmarsh flow, tracer movement, and residence time
- Salt marsh DEMs must resolve the length scale associated with hydraulic connectivity, but not the smallest intertidal creeks

Supporting Information:
- Supporting Information S1

Correspondence to:
J. C. Sullivan,
jessicasu@usca.edu

Citation:
Sullivan, J. C., Torres, R., & Garrett, A. (2019). Intertidal creeks and overmarsh circulation in a small salt marsh basin. *Journal of Geophysical Research: Earth Surface*, *124*, 447–463. https://doi.org/10.1029/2018JF004861

Received 5 SEP 2018
Accepted 21 JAN 2019
Accepted article online 25 JAN 2019
Published online 9 FEB 2019

Abstract The role of intertidal creek networks in overmarsh circulation is not well constrained. In this study, we systematically remove intertidal creeks from a high-resolution salt marsh digital elevation model and conduct new flow simulations with each iteration. Overall, removal of first- and second-order creeks reduced drainage density by 65%, and this had a negligible effect on overmarsh circulation and tracer distribution. However, upon removal of third- and fourth-order creeks, drainage density was reduced by 80% of the original value, and changes in peak velocity magnitude across various spatial and temporal scales reveal a system-wide switch from ebb to flood dominance. This response coincides with the interruption of topographically connected creeks that facilitate the direct exchange of water and tracer between the marsh interior and the larger subtidal system. Further, this reduction in hydraulic connectivity gives rise to less expansive tracer dispersal and a systematic decline in tracer residence time. Together, these results reveal that for the Groves Creek marsh, lower-order intertidal creeks have a minor role in overmarsh circulation, while higher-order creeks increase the potential for short circuiting of flow; they greatly influence overall flood and ebb dominance, and net tracer dispersal and associated retention time. Results reported here provide new insight on, for example, salt marsh restoration and the requisite digital elevation model bathymetry for robust simulations of overmarsh circulation.

1. Introduction

Intertidal creeks are ubiquitous features of salt marsh landscapes, and they have long been assigned a major role in salt marsh morphodynamics as conduits for material exchange (e.g., Allen, 1992; Esselink et al., 1998; French & Spencer, 1993; Leonard, 1997; Pestrong, 1965; Pethick, 1984; Reed et al., 1999). For instance, field studies indicate that the variable density of intertidal creeks greatly influence the distribution and characteristics of particulate organic matter (Chen et al., 2016; McLeod et al., 2012). On the other hand, field and numerical studies indicate that intertidal creek flows have a minor role in broader overmarsh circulation. For instance, Dankers et al. (1984) noted that tidal exchange over the marsh edge has a considerable influence on the transport and fate of particulate and dissolved material. In another study, French and Stoddart (1993) found that about 39% and 47% of the tidal prism flowed over the marsh edge on flood and ebb, respectively, with flows transitioning from topographically influenced to hydraulically controlled over the tidal cycle. Hence, overbank flows, but not necessarily intertidal creeks, are major components of salt marsh tidal exchange. Similarly, the work of Shaw et al. (2016) revealed that for a microtidal, river-dominated system, overbank flows, rather than creeks and channels, are the primary mechanism for water delivery to the marsh interior.

Modern technology allows for the rapid acquisition of large swaths of topographic-bathymetric data that facilitate studies of flow processes. However, the variable density of these data has led to questions about how digital elevation model (DEM)-bathymetric inaccuracies might affect the representation of subtle topographic features and, therefore, the assessment or estimates of flow at the ocean bed (Maleika, 2015), terrestrial channels (McKean et al., 2014), and for estuarine landscapes. For the latter, Cea and French (2012) found a strong response in current velocity to bathymetry, while water level fluctuations were influenced more by bed friction of a shallow estuary. Also, Camacho et al. (2014) performed uncertainty analyses of velocity for 3-D hydrodynamic simulations, and they documented discrepancies in current velocity and salinity for locations where DEM depths underpredicted observed elevations.

These findings contrast with the results of Temmerman et al. (2005) who used a 3-D hydrodynamic-sediment transport model to assess the interactions of topography, vegetation, and water level fluctuations on spatial variations in flow and sedimentation. Their 0.05-km^2 flow domain came from a lidar DEM reduced to 3-m point spacing and with a vertical accuracy of ±0.13 m. Hence, surface depressions and creeks that were less than 3 m wide or of decimeter scale relief were not highlighted in the flow domain. Despite this apparent limitation, the model validation was robust, leading the authors to conclude that topography has a nominal effect on flow and sediment transport relative to the influence of vegetation and tides. More recently, Falcao et al. (2013) investigated the influence of bathymetric interpolation errors on intertidal flooding. They found that vertical offsets of <0.25 m had no effect on the computation of water level and inundation extent during high water but found discordance at low tide.

Recently, Blanton et al. (2010) simulated tracer circulation and retention in a mesotidal salt marsh. Comparisons between observed and simulated discharge, axial velocity, and water level reveal that the model successfully replicated the hydrodynamic processes of relatively large subtidal channels. However, the modeled tracer distributions were less robust in that, for instance, the model failed to replicate peak tracer concentrations at the outer extent of the basin. These results led the authors to speculate that contaminant dispersal and retention, and overall salt marsh circulation, are highly sensitive to geomorphic structure, particularly flows through small-scale intertidal creeks unresolved in the lidar bathymetry. In other words, Blanton et al. (2010) implied that first-order creek systems facilitate greater overall salt marsh circulation. Later, the same site was surveyed in high detail using a real-time kinematic global positioning system, and Sullivan et al. (2015) used the resulting DEM in simulations of overmarsh flow. They showed highly complex flow patterns in both space and time, and they associated this response with the submergence/emergence of decimeter-scale topography. Moreover, they found that the complex flow patterns were not necessarily related to flows through creek networks. The disparate findings from this set of studies collectively show that the hydraulic interactions among creek flows and overall marsh circulation are not well constrained.

Here we ask the following: What is the effect of intertidal creeks on the temporal and spatial variability in patterns of tidal circulation in and around salt marsh systems? We address this question by systematically removing intertidal creeks from the high-resolution, high-accuracy DEM of Sullivan et al. (2015) and conducting corresponding flow simulations. An ancillary benefit of this work arises from the fact that it provides deeper insights into the level of topographic detail required for accurate flow simulations in salt marsh environments; it sheds light on, for example, the level of creek system detail necessary for restoration of surface water flows in disturbed or reconstructed salt marsh systems. Overall, we report the effects of creek removal on flood/ebb dominance of peak velocity magnitude, tracer dispersal, and associated residence times, all being metrics relevant to material exchange (e.g., carbon sequestration), restoration, and contaminant cycling in salt marshes. This work is driven by the following hypothesis: Small-scale intertidal creeks have a small role in overmarsh circulation.

2. Study Site

The Groves Creek study site is a 1.4-km^2 section of a larger salt marsh system ~20 km south of Savannah, Georgia, USA (Figure 1a). The basin is partially enclosed by a 1- to 3-m bluff at the forest-marsh boundary along the west and south. To the north the site is bound by Groves Creek, a sinuous, 3.2-km-long subtidal channel with a ~100-m-wide mouth open to the Wilmington River, ~11 river kilometers from the coastal ocean (Figure 1a). At 3.1-km upstream of the mouth, Groves Creek narrows to about 40 m where it splits into three branches, West, Middle, and East, with lengths of 1.4, 0.7, and 0.5 km, respectively (Figure 1a). Together, Groves Creek and the branches constitute the subtidal system with maximum depth of 4.5 m at the mouth, to 1.2 m inland near the ~1-m-wide tips of the three branches proximal to the terrestrial edge (Figure 1b). The entire subtidal system accounts for 0.16 km^2 or about 11% of the study area. The eastern boundary has moderate channel development that is susceptible to inundation directly from the subtidal Wilmington River (Figure 1b).

A manual perimeter trace around the subtidal system reveals 165 intertidal creeks or conduits with "v"- or "u"-shaped mouths that intersect Groves Creek with mouth top widths greater than 5 m, mouth bed elevations ranging from −0.79 to 0.20 m, a mean elevation of −0.16 m ± 0.26 m (Figure 1b). All elevations are reported relative to the North American Vertical Datum – 1988 (NAVD88). Spacing between creek mouths ranges from 4 to 300 m with an average of 47 m ± 54 m (Figure 1b). The larger spacing occurs along the

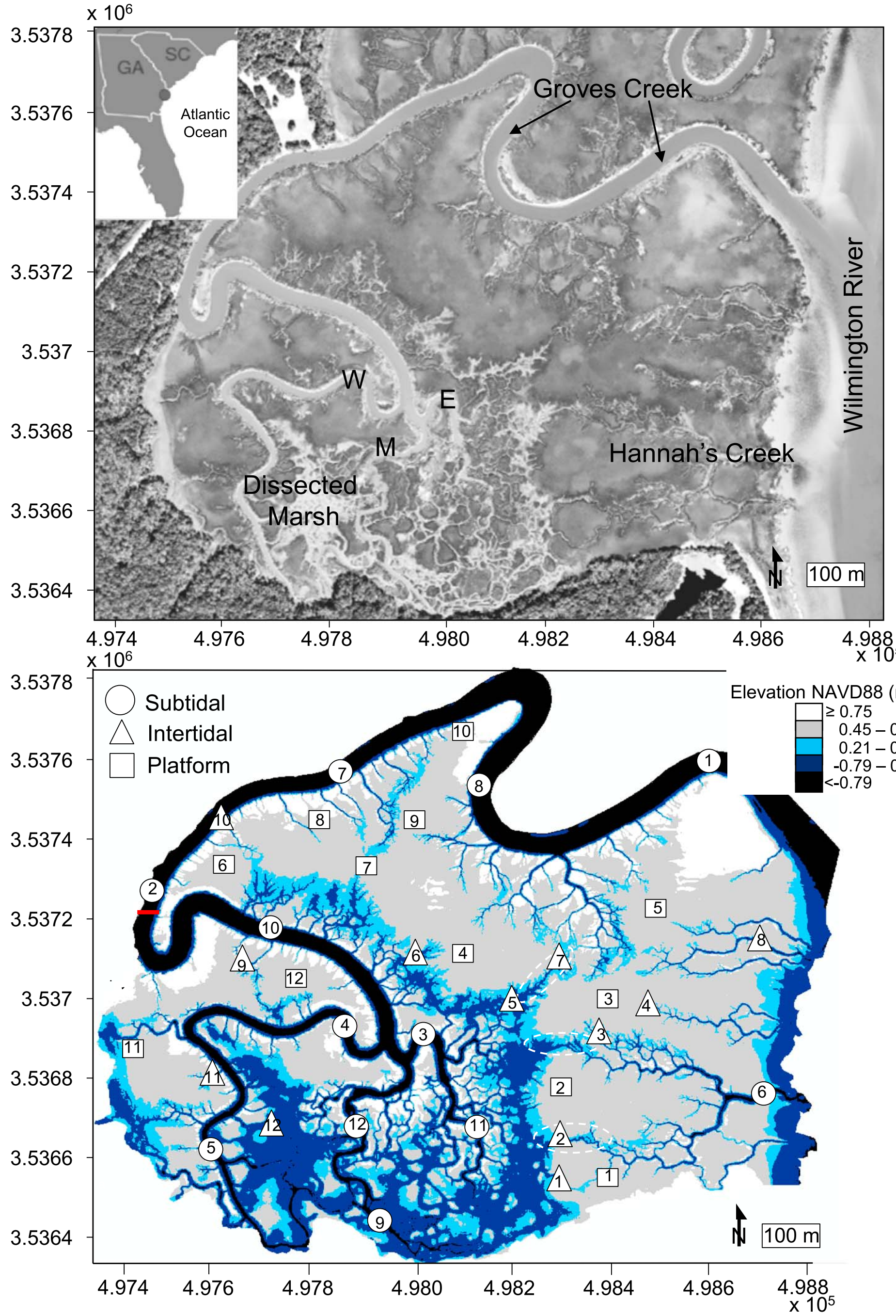

Figure 1. (a) Groves Creek is a semienclosed creek-marsh system located approximately 20 km south of Savannah, GA, USA. Groves Creek has three subtidal branches labeled E, W, and M for East, West, and Middle, respectively. (b) The high-resolution reference digital elevation model is shown. White, gray, light blue, dark blue, and black areas represent levee, platform, surface depressions, intertidal creeks, and subtidal channel, respectively. Also shown are the 36 at-a-station sites for monitoring the velocity residuals for subtidal (circles), intertidal (triangles), and platform (squares) locations. Dashed, white ellipses highlight locations where intertidal creeks and surface depressions form direct connections between the marsh interior and the Wilmington River. The small red line near station 2 marks the location of the tracer release.

meanders of Groves Creek and tighter spacing along straight reaches (Figure 1b). The maximum along-creek lengths are highly variable, ranging from 4 to 550 m, with an average of 74 m ± 89 m (Figure 1b). Creek mouth widths vary from <1 to 20 m, with narrower creeks typically found in the northern areas

10.1029/2018JF004861

(Figure 1b). In particular, most of the narrow, relatively short and straight creeks occur along the first 2.3 km of Groves Creek, and these features tend to dissect well-defined levees (Figure 1b). To the east along the Wilmington River, the longest and deepest creeks cross the marsh edge (Figure 1b) and are approximately normal to the river. The longest is Hannah's Creek (Figure 1a) at 550 m, becoming narrower and shallower upstream, going from 14 to 4 m, and with −1.2 to 0.09 m bank full elevations, respectively (Figure 1b). This creek provides a conduit for flows between the basin interior and the Wilmington River (Figures 1a and 1b).

Within the marsh interior, some creeks form complex networks that are connected at their heads by surface depressions (Figure 1b). In particular, creeks along and at the heads of the subtidal branches form a distinct system of reticulated or circular creeks that define small intertidal islands (<500 m^2). These creeks dissect a large 0.24-km^2 depression in the southeast, hereafter referred to as "dissected marsh," which has a mean elevation of −0.52 m (Figures 1a and 1b). Hence, the Groves Creek salt marsh has two types of intertidal creek systems, reticulated and branching, contained by 0.24 and 1.16 km^2 subbasin areas, respectively; Strahler stream ordering was applied to the latter. Collectively, the intertidal creek systems occupy 19% of the study area.

Higher in the tidal framework are the surface depressions, sparsely vegetated areas between 0.21 and 0.44 m with a mean elevation of 0.34 m ± 0.07 m. These depressions occupy 0.18 km^2, or 13% of the basin (Figure 1b). Contiguous surface depressions form an arc-shaped trough paralleling Groves Creek and connect the heads of several creek networks (Figure 1b). The position and orientation of these low-lying areas facilitate early and far-reaching inundation, and late and prolonged drainage on ebb (Sullivan et al., 2015).

Still higher in the tidal framework is the marsh platform comprising 0.64 km^2, or 46% of the study area. This expanse of vegetated, low-relief area occurs between 0.45 and 0.74 m with a mean elevation of 0.61 m ± 0.07 m (Figure 1b). Intertidal creeks and surface depressions divide the landscape into smaller isolated subplatform areas, particularly to the north and east of the marsh interior (Figure 1b). In particular, there are three locations where creeks and surface depressions form troughs that cut across the marsh platform and form direct links to the subtidal system (Figure 1b). The first is located ~0.6 km north of the terrestrial border (Figure 1b) and connects the marsh interior to Groves Creek. Two others occur at the head of Hannah's Creek and connect the marsh interior to the Wilmington River (Figures 1a and 1b).

The highest areas comprise sets of discontinuous levee that occupy 10% of the basin and reach 0.75 to 1.30 m. The local relief along levees is about 0.40 m, and the mean elevation is 0.85 m ± 0.07 m (Figure 1b). Most levees along the first 2 km of Groves Creek vary in height and width but are typically crosscut by intertidal creeks (Figure 1b). Smaller, isolated levees tend to form along the banks of the subtidal branches, and along the banks of the larger creeks; see for instance position 3.537×10^6, 4.978×10^5 on Figure 1b.

The vegetation is a monoculture of the smooth cordgrass *Spartina alterniflora* (*S. alterniflora*) with spatial variations in density and height dependent on surface elevation (Alexander et al., 2017; Sullivan et al., 2015). For instance, tall *S. alterniflora* has stem heights that exceed 2 m and a stem density of about 112 stems per square meter that grows on the high channel banks and levees. The short form, which typically occurs on the marsh platform, has an average stem height of 0.28 m and a stem density of about 446 per square meter. These values are based on clippings from 1-m^2 quadrats at an off-site location.

3. Methods

3.1. Model Description and Setup

The area experiences a mixed, semidiurnal, ebb-dominant local tidal regime (Blanton et al., 2010). The system has a typical spring tidal range of 3.2 to 3.8 m, while neap tide range is 1.2 to 1.5 m. This modeling study corresponds to a 5-day period between 31 October and 5 November 2010. During this interval, the tidal range varied from 2.1 to 3.2 m, and during high-high tide conditions the mean water depth over the marsh platform was ~1 m, and the entire basin was submerged.

Here we used the validated model of Sullivan et al. (2015), which uses a 2-D depth-averaged finite difference numerical scheme for hydrodynamic simulations (Delft3D run in 2-D mode; e.g., Lesser, 2000). The simulation approach consists of integrated modules that compute water currents, water quality, and particle transport. The standard hydrodynamic module is Delft3D FLOW, and it accurately simulates flows where horizontal length scales are significantly larger than the vertical (Lesser, 2000). It relies on a finite

10.1029/2018JF004861

difference approach to compute water level and depth-averaged velocity at each node. The output was subsequently coupled to the PART module to simulate the advection and diffusion of a tracer. The PART module of Delft3D provides a detailed description of concentration distributions, resulting from instantaneous or continuous releases of salt, oil, temperature, or other conservative or simple decaying substances by means of a particle-tracking method using the 2-D (or 3-D) flow data output from the FLOW module (Delft3D-FLOW UM, 2013; Van den Boogaard et al., 1993). PART is based on the principle that the movement of particles in water can be described in three dimensions, whereby a dynamic tracer concentration is obtained by calculating the mass of particles in each computational grid cell. The PART module uses a random walk approach where the movement of particles results from advection due to currents, and from the random movement of particles related to the horizontal dispersion coefficient H_D (Csanady, 1973), where

$$H_D = at^b, \tag{1}$$

and t is the length of time that a particle of water stays in the system, and a and b are dispersion coefficients that influence the time variation of the random spreading process and emerge from model calibration (Bent et al., 1991). For these 2-D flow simulations, a roughness length parameter of 0.001 m was specified (Nepf & Ghisalberti, 2008; Raupach, 1994; Sullivan et al., 2015), and this in turn helped determine the logarithmic vertical velocity profile.

Flow was simulated on a grid of 1-m horizontal spacing with 5.2×10^6 computational nodes. A computational time step of 1.5 s was used to establish numerically stable simulations, and results were output at 10-min intervals. The domain was closed to the west and south along the terrestrial border and closed to the north along the outer bank of Groves Creek. The domain was open to flow along the eastern boundary defined by the observed water level time series from subtidal station 1 (Figure 1b).

The horizontal eddy viscosity was set to 0.0005 m^2/s (Temmerman et al., 2005), and bottom roughness was applied as two spatially variable Manning n values of 0.10 and 0.017 for vegetated and unvegetated marsh, respectively, that follow from model calibration described in Sullivan et al. (2015). These values are comparable to the range of published salt marsh values reported in the literature (see Sullivan et al., 2015) and yield excellent agreement between observed and simulated water levels as shown by the model efficiency of 0.99 ± 0 for water level, 0.89 ± 0.04 for depth averaged velocity, and 0.57 ± 0.22 for tracer concentrations (Sullivan et al., 2015).

Due to the stochastic nature of the dispersion process, the tracer simulation required a large number of particles to obtain the best results. Here the modeled dye tracer consisted of 7.0×10^6 particles, a compromise between achieving high accuracy and maintaining computational efficiency. The accuracy of the tracer simulation was set as the lowest concentration that can be represented by a single particle in a computational cell; in this case 4 ppb. Horizontal dispersion parameters were set to $a = 0.20$ $m^2/s^{(1+b)}$ and $b = 0.02$ (Sullivan et al., 2015).

3.2. Characterization of Creek Networks and Model Scenarios

The high-resolution DEM of Sullivan et al. (2015) is referred to as the *reference*. The creek networks corresponding to the reference were identified and ordered according to Strahler (1952) by the following approach. Creek lines were generated from the reference using the hydrology tools in ArcGIS 10.3 software (sensu Tarboton et al., 1991), which is a widely accepted, well known method that has been successfully applied to salt marsh landscapes (e.g., Lawrence et al., 2018; Vandenbruwaene et al., 2012, 2013). Additionally, a minimum creek depth of 0.10 m was specified to limit the extent of first-order creeks. Overall, this approach was successful in identifying creeks and creek networks, and the resulting creek map was used to estimate the total length and average mouth width of each creek order. This method did not work for the reticulated drainages of the dissected marsh; therefore, creek lines within this area were generated manually. We then tested the model sensitivity to reticulated drainages by manually removing all points from the reference and a revised DEM was generated. The net result was a DEM with reticulated drainage “filled in.” Spatial variations in hydrodynamic roughness coefficients corresponding to the revised surface were updated using the criteria for unvegetated and vegetated conditions described above. The DEM with filled in reticulated drainages was applied to flow and tracer simulations, and the resulting residual velocities, tracer circulation, and residence time were compared to the reference simulation (details provided therein).

The branching creek networks identified with the Tarboton approach were sequentially removed from the DEM by filling in the upstream parts of creek networks up to the desired Strahler order (Figure 1b). The net result was a straightening of the local contours. Further, estimates of average mouth width provided criteria to constrain the filling process. In this case, we took the average mouth width for first-order creeks as 4 m; all elevation points within 4 m of first-order creek lines were removed. This process was applied sequentially to remove parts of creek networks through Strahler order 4. Order 5 creeks fell within the subtidal range of elevations and were not included in the creek removal process. Note, with removal of each creek order, a new DEM was generated and new roughness values were assigned to filled in areas that conceptually transitioned from intertidal muddy creek bed and bank to salt marsh platform, or from unvegetated to vegetated conditions. We then conducted simulations of overmarsh flow and tracer circulation for each altered surface.

Changes imparted to the landscape by the above methods were quantified using drainage density. The drainage density, *Dd*, for each surface was calculated as the ratio of total creek length to total basin area, 1.4 km^2 (e.g., Marani et al., 2003; Vandenbruwaene et al., 2012). One important outcome of the creek removal process was the apparent disruption of conduits linking intertidal creeks and marsh interior. Overall, the numerical simulations conducted over the sequence of altered DEMs provided a geomorphic context for assessing the role of intertidal creeks in overmarsh circulation, with drainage density and geomorphic-hydraulic connectivity as independent variables. Here we defined hydraulic connectivity as intertidal creek networks that are topographically connected, thereby facilitating direct exchange of flows between the marsh interior and the larger subtidal system (Ashley & Zeff, 1988).

3.3. Overmarsh Circulation

We assessed the effects of creek removal on overmarsh circulation at various temporal scales and at a range of locations. Simulation monitoring stations were selected for subtidal, intertidal, and platform areas using random sampling in ArcGIS. A threshold spacing of at least 100 m was chosen based on the approximate length scales of flow complexity within the marsh interior (Sullivan et al., 2015) and on the pathways that facilitate hydraulic connectivity (Figure 1b). In the subtidal area, there were six random sites and the six monitoring sites of Sullivan et al. (2015). Further, there were 12 random stations from the intertidal and platform areas, 36 in total. For each station, the peak velocity residual, *Rpv*, was computed per tidal cycle as

$$Rpv = vebbMAX – vfloodMAX, \tag{2}$$

where *vebbMAX* and *vfloodMAX* are the peak ebb and flood velocity magnitude, respectively, and *Rpv* was used as an indicator of flood or ebb dominance. For instance, a stronger peak ebb magnitude yields a positive *Rpv*, and we take this to represent ebb dominance (e.g., Austin et al., 2009), which is a first-order indicator of the preferred direction of water fluxes (Austin et al., 2009; Brown & Davies, 2010; Cavalcante, 2015; Dronkers, 1986; Friedrichs & Perry, 2001; Jewell et al., 2012; Lincoln & Fitzgerald, 1988). Likewise, a stronger peak velocity magnitude during flood will yield a negative *Rpv*, or flood dominance. An *Rpv* of zero indicates balance between peak ebb and flood velocity magnitude. For each simulation, *Rpv* for each station and for each tidal cycle was computed. The mean *Rpv* for subtidal, intertidal, and platform areas was compared to the reference. This approach was useful because it provided an unbiased assessment of how creek removal influences system wide tidal current dominance and enabled a local-scale evaluation of water circulation.

3.4. Tracer Circulation

Conservative tracer distributions were simulated as an instantaneous source released 60 m south of subtidal station 2 (Figure 1b) at 16:00 UT, or 2 hr after low tide, on 1 November, coincident to the location of an earlier dye release (Sullivan et al., 2015). For each creek removal scenario the modeled tracer circulation was compared to the reference flow conditions. In particular, we evaluated the effects of creek removal on the spatial distribution of tracer at 2 hr before and after high tide of the tidal cycle subsequent to the tracer release. Also, the standard distance of particles, *SD*, (e.g., Mitchell, 2005; Shahriari & Blumsack, 2017) was computed as

$$SD = \sqrt{\frac{\sum_{i=1}^{n} (x_i - \overline{X})^2}{n} + \frac{\sum_{i=1}^{n} (y_i - \overline{Y})^2}{n}}, \tag{3}$$

where x and y are the coordinates of each tracer particle, i; $\overline{X}$ and $\overline{Y}$ represent the mean center of all particles (i.e., center of tracer mass); and n is equal to the total number of particles, to provide a measure of tracer dispersal. Next, the time series of the total tracer mass in the basin was used to quantify changes in residence time for each simulation. Residence time, *Rt*, is defined as the time it takes for the initial tracer mass within the basin to become diluted 63% with water from the Wilmington River (e.g., Arneborg, 2004; Gillibrand, 2001; Monsen et al., 2003) and represents the 1/e threshold approximation of the pulse residence time relative to the injection point (e.g., Viero & Defina, 2016).

4. Results

4.1. Creek Order, Creek Removal, and Drainage Density

Removing the reticulated creek system from the DEM had negligible effect on simulation results when compared to the reference condition. For instance, there was a <0.05% change in all metrics after the removal (see Tables S2 and S7 for details). Hereafter, for computational efficiency all flow simulations are conducted without the reticulated system. The branching intertidal creek systems have a maximum Strahler order 5 (Figure 2), and total creek length per Strahler order declines quasi-exponentially from order 1 to 5 (Table 1), consistent with other salt marsh networks (e.g., Novakowski et al., 2004; Ragotzkie, 1959). Therefore, simulations conducted on the progressively smoother land surface in fact have ~50% of the creeks removed with each iteration of "in-filling" and the total marsh area affected by each iteration also declines exponentially.

The first manipulation of the reference DEM was to fill in the reticulated and order 1 creeks; the total creek length goes from 30.5 to 15.4 km, and *Dd* from 21.7 to 11.0 km/km^2 (Table 1). Removal through order 2 reduces *Dd* to 7.6 km/km^2 (Figure 3b). Removing orders 1–3 gives *Dd* of 5.7 km/km^2. At this level of smoothing the surface depressions that connect the marsh interior to the dissected marsh persist, but the conduits connecting the marsh interior to Hannah's Creek are not detectable (Figure 3c). With the removal of orders 1–4 the *Dd* is 4.7 km/km^2, and parts of the system appear as closed basins. In the following sections, the effects of creek removal on overmarsh circulation are shown as comparisons of the results in response to the removal of orders 1 through 2, and 1 through 4, hereafter referred to as "1–2" and "1–4," respectively, relative to the reference conditions.

4.2. At-a-Station Velocity

The peak velocity residuals, *Rpv*, computed for the reference and the creek removal scenarios at the 36 stations are listed in Tables S1–S6. The spatial context is given by references to Figure 1b. In the subtidal part of the system the reference residual velocity, *Rpv*, varies from 0.01 to 0.62 m/s, and the mean is 0.16 m/s ± 0.11 m/s. The lower residuals occur in the East and Middle branches (stations 3, 9, 11; Figure 1b), while the higher values occur near the eastern marsh edge (station 6; Figure 1b). For 1–2 the range is 0.01 to 0.45 m/s with a mean of 0.17 m/s ± 0.07 m/s, with the high and low values in Groves Creek and at eastern marsh edge, respectively. At 1–4, there is a mix of negative and positive values that range from −0.22 to 0.68 m/s, but the overall mean is positive, 0.18 m/s ± 0.19 m/s. The negative values are in the Middle and East branches of Groves Creek (stations 9, 11, and 12; Figure 1b).

The intertidal areas contain *Rpv* values that range from 0.01 to 0.45 m/s, with a mean of 0.07 m/s ± 0.08 m/s. Lower values occur in the marsh interior (stations 1, 5, 6, and 12; Figure 1b), while the highest occur near the Wilmington River (station 8; Figure 1b). With 1–2 the response is variable; negative and positive values range from −0.01 to 0.44 m/s, but the mean is positive: 0.05 m/s ± 0.04 m/s. The negative and positive values correspond to the marsh interior (stations 1, 3, and 12; Figure 1b) and the area near the Wilmington River, respectively. For 1–4, *Rpv* is negative at all intertidal stations, ranging from −0.01 to −0.14 m/s with a mean of −0.02 ± 0.02 m/s. The platform values are consistently positive in the reference scenario, ranging from 0.00 to 0.03 m/s with a mean of 0.01 ± 0.005 m/s. The 1–2 values range from −0.01 to 0.03 m/s, but the overall mean is 0.00 m/s ± 0.02 m/s. With 1–4, *Rpv* is negative at all 12 platform sites, ranging from −0.01 to −0.07 m/s with a mean of −0.02 m/s ± 0.002 m/s.

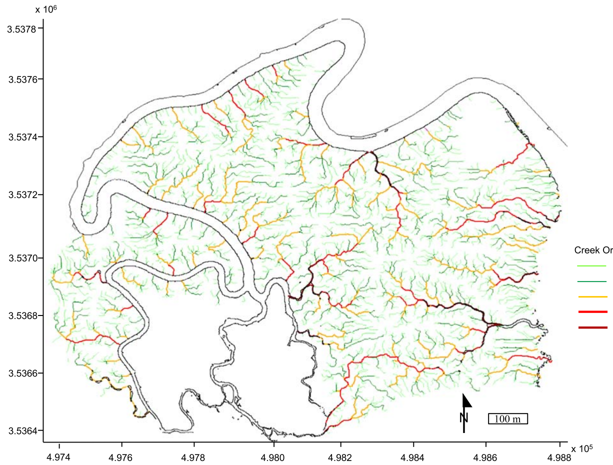

Figure 2. Strahler creek order for the Groves Creek basin ranges from 1 to 5. Digital elevation model points associated with reticulated (colored white) creeks and those through Strahler order 4 were systematically removed to produce a series of altered digital elevation models.

Altogether, the reference *Rpv* values are consistently positive at all 36 stations, and the same is true for the 1–2 scenario. However, for the 1–4 case, the subtidal response shows a mix of negative and positive values, and *Rpv* values at all intertidal and platform sites are negative. Overall, the mean *Rpv* values reported in this section are equal to or greater than the standard deviation and are, therefore, representative of residual peak velocity conditions across the 5-day record.

The regression plots in Figures 4a and 4b provide a comparison of the at-a-station response to creek smoothing. A 1:1 correspondence indicates no response while points above or below the line indicate deviation from the reference condition. In particular, the figures show that continued smoothing may cause the residuals to shift from positive to negative, indicating a change to flood dominance (Austin et al., 2009; Cavalcante, 2015; Friedrichs et al., 1990; Jewell et al., 2012). For the reference and 1–2 conditions (Figure 4a) the system-wide response indicates ebb dominance, and the correlation coefficients, R^2, of 0.53, 0.86, and 0.88 for subtidal, intertidal, and platform sites, respectively, reveal only moderate to slight deviation from the reference. However, for 1–4 (Figure 4b) three of the 12 subtidal stations became flood dominant, and these sites are associated with the branches of Groves Creek. Further, all intertidal and platform stations plot below the 1:1 line ($R^2 = -0.89$ and 0.51, respectively), indicating that the 1–4 case produces a consistently stronger peak for flood conditions relative to ebb. In other words, this level of creek infilling gives rise to a switch from ebb to flood dominance for 92% of the 36 stations.

4.3. Tracer Circulation

4.3.1. Tracer Dispersal—Flood (2 Hours Before High Tide)

Maps of tracer distribution correspond to conditions of the first full tidal cycle following the tracer release. The reference distribution shows a 2-km-long half oval shaped front of 100–500 ppb open to the northwest, centered on Groves Creek (Figure 5a); the southern reach of the front is set by the flow boundary. Several features interrupt this general view: First, there are ≤0.013-km^2 pockets of 300–500 ppb in the dissected marsh area. Second, there is a 0.02 km^2 area 0.1 km east of the dissected marsh where tracer concentrations are 50–100 ppb. Third, there are ≤0.02-km^2 pockets of 200–300 ppb near the upper reaches of Hannah's Creek (Figure 5a).

Table 1
Summary of Total Length (km), Average Mouth Width (m), and Elevation (m) for Reticulated Drainage and Orders 1, 2, 3, 4, and 5 Creeks and Groves Creek

	Reference length (km)	% of total creek length	Average mouth width (m)	Average mouth elevation (m)	Length (km) remaining: Reticulated removed	Length (km) remaining: Order 1 removed	Length (km) remaining: Order 2 removed	Length (km) remaining: Order 3 removed	Length (km) remaining: Order 4 removed
Reticulated drainage	3.4	11.1	n/a	n/a	0	0	0	0	0
Order 1	11.7	38.4	4.4 +/− 2.9	0.38 +/− 0.35	11.7	0	0	0	0
Order 2	4.8	15.7	5.9 +/− 2.7	0.25 +/− 0.32	4.8	4.8	0	0	0
Order 3	2.6	8.5	7.64 +/− 2.9	0.04 +/− 0.30	2.6	2.6	2.6	0	0
Order 4	1.4	4.6	10.54 +/− 4.1	−0.15 +/− 0.34	1.4	1.4	1.4	1.4	0
Order 5	0.6	2.0	16.1 +/− 2.8	−0.91 +/−0.16	0.6	0.6	0.6	0.6	0.6
Groves Creek	6.0	19.7	29.2 +/− 20.9	−2.6 +/− 0.91	6.0	6.0	6.0	6.0	6.0
Total creek length (km)	30.5	n/a	n/a	n/a	21.7	15.4	10.6	8.0	6.6
Dd (km/km^2)	21.7	n/a	n/a	n/a	19.3	11.0	7.6	5.7	4.7

Note. The table highlights the change in total creek length and associated *Dd* (km/km^2) for each creek removal scenario (gray-highlighted rows).

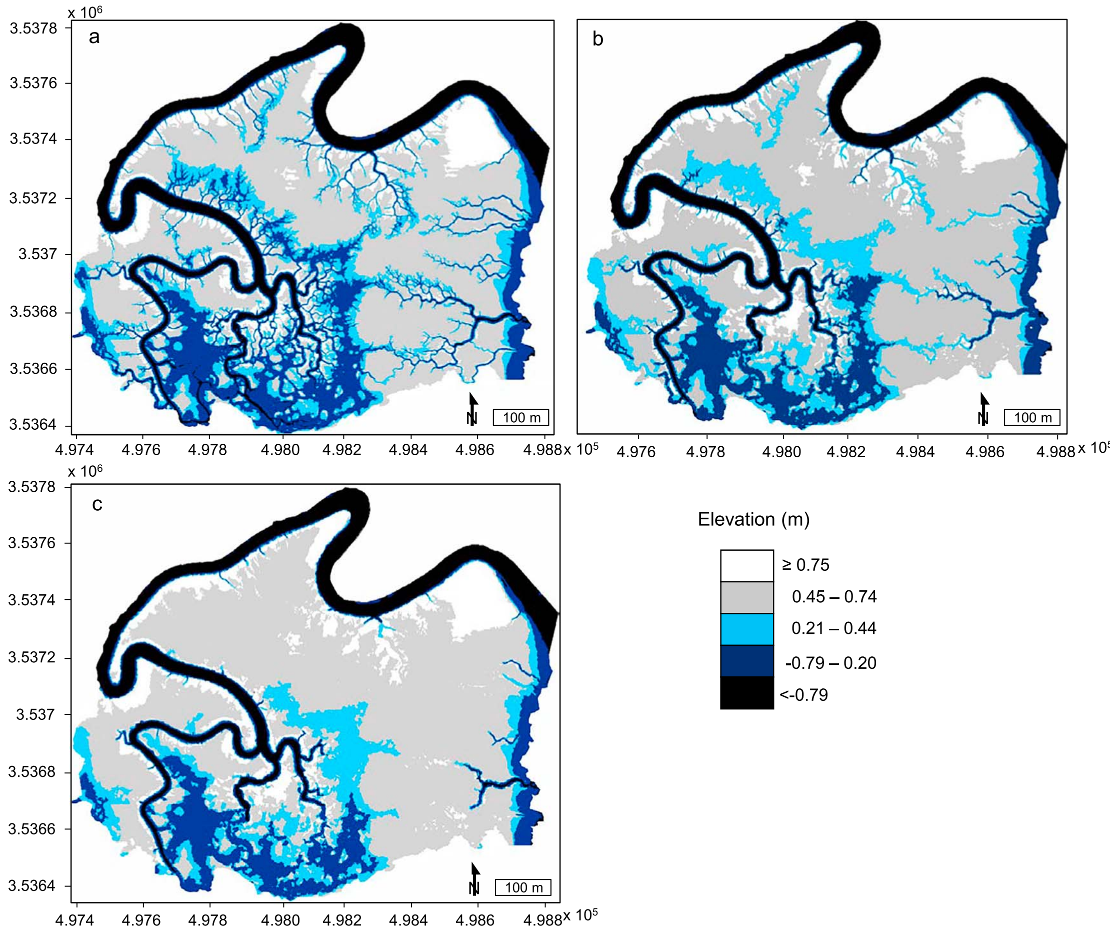

Figure 3. The (a) reference, (b) 1–2, and (c), 1–4 digital elevation models are shown. From high to low elevation, the contour intervals reflect the elevation range of levees (white), marsh platform (gray), surface depressions (light blue), intertidal creeks (dark blue), and subtidal channel (black). The series of digital elevation models highlight (b) the removal of small, lower-order creeks and (c) the disruption of topographically connected conduits that enable flow short-circuiting once higher-order features are removed.

The general distribution for 1–2 is similar, but with higher concentration areas shifted eastward, and with a continuous, 500-m-long, and 0.03-km^2 swath of 500 ppb near the heads of Hannah's Creek (see for instance 3.5368×10^6, 4.982×10^5 m in Figure 5b). At 1–4, concentrations range from 100 to 500 ppb with up to 300 ppb along the northern reaches of the front (3.5372×10^6, 4.98×10^5 m) and as much as 500 ppb within the southern limits of the basin (Figure 5c). Specifically, there is a 700-m-long, 0.035-km^2 swath of 500 ppb extending from the dissected marsh to ~60 m west of Hannah's Creek (Figure 5c).

Comparisons between the reference and 1–2 scenario show slightly enhanced tracer dispersal (Figure 5b), and a 4% increase in *SD* (Table 2). Moreover, the areas of 500 ppb are shifted eastward relative to their initial position, and, in particular, there is a more extensive reach of high concentration near Hannah's Creek (Figure 5b). On the other hand, with 1–4 the tracer is less disperse throughout (Figure 5c), with a 26% decrease in *SD* (Table 2). Also, the tracer is more concentrated along the northern reach of the front, and high concentrations are largely confined to the marsh interior. Furthermore, less tracer occurs at the head of Hannah's Creek (Figure 5c). Taken together, these observations show that removal of smaller, lower-order creeks causes slightly enhanced tracer dispersal, but that change is diminished when all but order 5 creeks are removed.

4.3.2. Tracer Dispersal—Ebb (2 Hours After High Tide)

At 2 hr after high tide (Figure 6a), reference concentrations range from <10 to 400 ppb. Most of the higher concentrations occur as ≤0.01-km^2 pockets along the terrestrial border and near higher-order creek networks, while the lower concentrations occur to the north (Figure 6a). The resulting distribution nearly

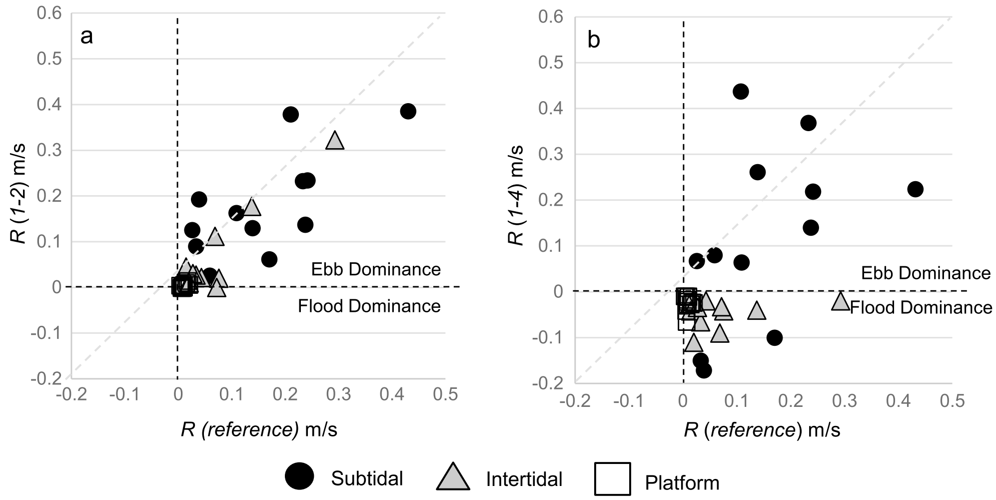

Figure 4. Regression plots used to compare at-a-station mean diurnal peak velocity residuals, *R*, resulting from the reference and (a) 1–2 and (b) 1–4 simulations. Note the overall switch to flood dominance at 1–4 (b).

encircles the inner part of Groves Creek, and the outward 1.5-km-long nonuniform front develops several "points" associated with focused flow away from the marsh interior and toward the small intertidal creek networks to the north (Figure 6a). Moreover, concentrations of up to 80 ppb occur beyond the mouth of Hannah's Creek (Figure 6a), while tracer appears to exit the system via Groves Creek.

At 1–2 the distribution is similar, with concentrations of ≤400 ppb and higher values largely associated with the southern border and the marsh to the east (Figure 6b), and a nonuniform front of ≤100 ppb along the

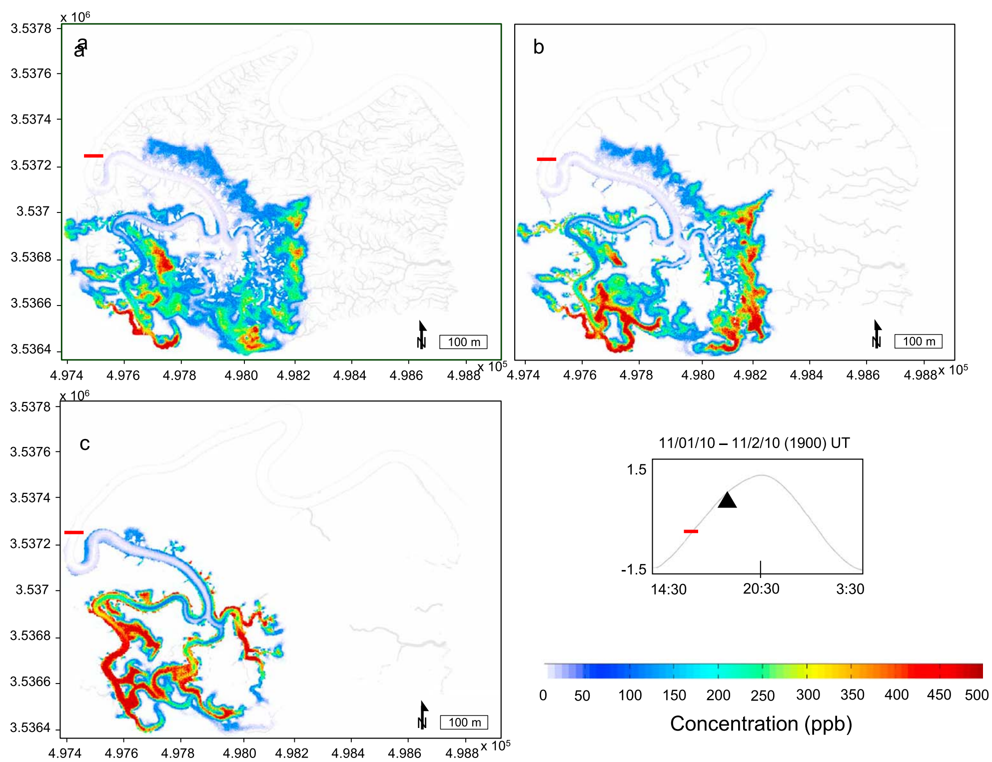

Figure 5. (a) Reference maps of simulated tracer dispersal 2 hr before high tide. Warm and cool colors show areas of high and low tracer concentration, respectively. (a) Reference simulation and (b) removing 1–2 order creeks result in slightly enhanced dye dispersal and higher concentrations shift eastward toward Hannah's Creek, while removing 1–4 order creeks (c) results in less dispersal to the marsh interior.

Table 2
Summary Table of Metrics Used to Describe the Effects of Creek Removal on Tracer Dispersal, SD (m), Percent of Tracer Remaining at the End of Each Tidal Cycle, and Associated Residence Time, Rt (days)

	Reference	1–2	1–4
SD, Flood (m)	310.61	323.30	230.48
SD, Ebb (m)	401.82	410.21	352.50
% tracer remaining (11 hr)	90	87	83
% tracer remaining (23 hr)	68	67	62
% tracer remaining (36 hr)	41	40	39
% tracer remaining (48 hr)	25	22	20
% tracer remaining (61 hr)	17	14	12
% tracer remaining (74 hr)	11	8	7
Rt (day)	1.86	1.75	1.59

marsh platform. Also, there is a plume of ≤100 ppb leaving Hannah's Creek, but no tracer leaves through Groves Creek (Figure 6b). With 1–4, concentrations are ≤500 ppb, and these high values occur as two pockets retained in the marsh interior, one 0.04 km^2 area along the southern terrestrial border at 3.537 × 10^6, 4.977 × 10^5 m (Figure 6c), and a second 0.03 km^2 region along the eastern marsh. At this time, no tracer leaves the system, but up to 20 ppb occurs within the main subtidal channel (Figure 6c).

Comparing the reference and 1–2 ebb scenario reveals that the tracer is slightly more disperse with a 2% increase in *SD* (Table 2) and the higher concentration center of mass is shifted eastward ~60 m relative to the reference (Figure 6b). Also, the tracer exiting the mouth of Hannah's Creek (Figure 6b) is more concentrated. However, 1–4 results in less dispersal with a 12% decrease in *SD* (Table 2), and higher concentration tracer remains in the marsh interior. Also with 1–4, no tracer leaves the system at 2 hr after high tide, and higher concentrated tracer appears within the main branch of Groves Creek (Figure 6c).

In summary, the tracer distribution at 1–2 is similar, albeit slightly enhanced relative to the reference. In particular, tracer is more disperse during flood, and higher concentration areas are shifted eastward. However, with 1–4 much more tracer is confined to the marsh interior, and there is less dispersal throughout the basin. On ebb, the reference and 1–2 scenarios show that the tracer primarily exits the system via Hannah's Creek, highlighting a short-circuiting of flows between the marsh interior and the Wilmington River. On the other hand, at 1–4 the tracer is confined to the marsh interior, less tracer passes through Hannah's Creek, and thus, Groves Creek assumes a larger role with respect water and tracer removal from the marsh interior.

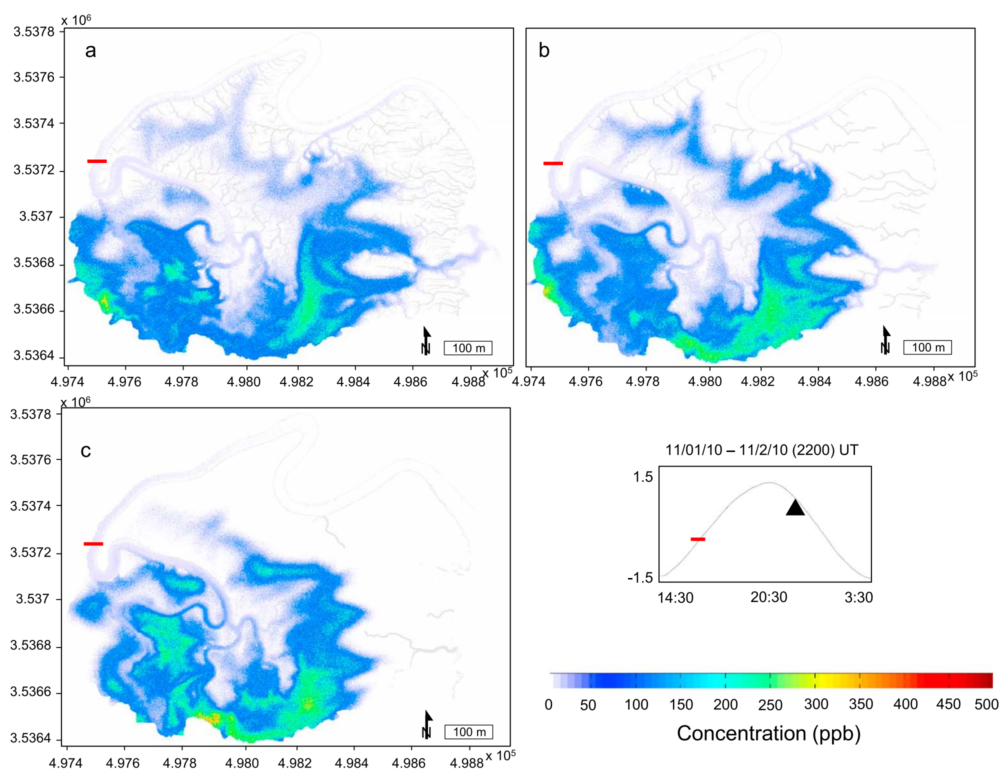

Figure 6. (a) Reference maps of simulated tracer dispersal 2 hr after high tide. Warm and cool colors show areas of high and low concentration, respectively. (a) Reference simulation and (b) removing 1–2 order creeks result in higher concentration areas shifted eastward, while (c) 1–4 produces dye retention in the marsh interior, no dye exiting Hannah's Creek, and higher concentration tracer in the main stem of Groves Creek.

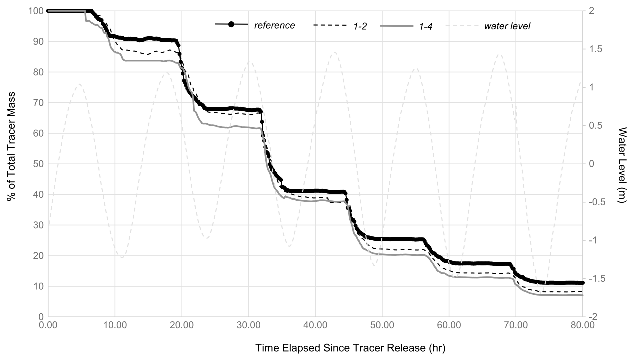

Figure 7. Time series of total tracer mass for reference, 1–2, and 1–4. All scenarios show the tracer mass declining exponentially with time after an initial lag.

Therefore, with respect to tracer circulation it appears that the intertidal networks facilitate greater subtidal exchanges.

4.3.3. Tracer Residence Time

Figure 7 shows the temporal trend of total tracer mass within the basin for the reference and creek removal scenarios. The reference curve demonstrates a roughly exponential decrease in total tracer mass with each passing tidal cycle after an initial lag. In particular, the initial mass declined by 10% at the end of the first tidal cycle (Figure 7; Table 2), followed by a ~40% decrease with each subsequent cycle (Figure 7). This level of exchange requires 1.86 days to reduce the initial tracer mass by 63%, with 11% remaining after 5 days (Table 2).

With 1–2, there is a 13% reduction after the first tidal cycle, followed by a ~40% decrease over the following tidal cycles (Figure 7; Table 2). The residence time, or time to 63% reduction, estimated from the tracer mass time series is 1.75 days (Table 2). After 8 days 5.1% of the initial tracer mass remains in the system (Table 2). With 1–4, 17% is removed after the first tidal cycle (Figure 7). As with the other cases, an exponential decline is apparent as ~41% removal with each tidal cycle (Figure 7). The residence time resulting from the 1–4 scenario decreases to 1.59 days (Table 2), with 7% of the initial tracer mass remaining in the system at the end of the 5-day period (Table 2).

Comparing the reference and creek removal scenarios reveals that in all cases, the initial tracer mass declines roughly exponentially after an initial lag, decreasing by ~40% with each tidal cycle. Overall, creek removal produces a systematic decline in tracer residence times for the Groves Creek salt marsh. In particular, with the removal of relatively small, lower-order creeks the tracer retention time is a 5% shorter. Likewise, removal of larger, higher-order creeks leads to a 14% reduction in tracer residence time, and 37% less tracer remaining in the system at the end of the 5-day period. Therefore, the role of intertidal creeks in tracer dispersal and retention is to facilitate wider dispersal and increased pathways for tracer exchange.

5. Discussion

The Groves Creek salt marsh is similar to other salt marshes in that small creek systems fill in much of the marsh interior and cut across levees or banks where they intersect the subtidal zone (Allen, 2000; Ashley & Zeff, 1988; Friedrichs & Perry, 2001; Leopold et al., 1993; Novakowski et al., 2004; Pethick, 1980). In this work, we assess the role of intertidal creeks in overmarsh circulation because they are ubiquitous features of salt marsh systems, but the length of time that they transmit water as conduits for open channel flows is in many cases negligible relative to the platform inundation. One product of systematically removing creeks through Strahler order 4 (of 5) and running flow simulations for each scenario was the revelation that higher-order creeks are associated with flow short-circuiting (e.g., different flood and ebb flow path lengths to larger subtidal sources) and influence numerical simulation of flood/ebb dominance and tracer dispersal much more than lower-order creeks. Specifically, we found that removing creeks through Strahler order 2, thus reducing the *Dd* by half, did not noticeably impact flows. On the other hand, removal through Strahler order 4 caused several of the short-circuiting features to be disconnected, and this had a notable effect on the properties of overmarsh circulation and tracer exchange across a range of spatial and temporal scales. We discuss both sets of results below.

The 1–2 case reduces *Dd* by 65%. Nevertheless, the overall response in *Rpv* across 36 random stations was negligible. In particular, in both the reference and the 1–2 scenarios there was a stronger peak ebb velocity relative to flood, or ebb dominant conditions. Further, the 1–4 scenario reduces *Dd* by 80%, and the topographic conduits that link flows between the marsh interior and the Wilmington River are broken. In response, the overall *Rpv* from 33 of the 36 monitoring stations indicate a switch to flood-dominant conditions. Together, these results reveal the following: (1) overmarsh circulation at various temporal and spatial scales is sensitive to the geomorphic representation of the landscape, and in particular to the degree of hydraulic connectivity of the marsh landscape. Moreover, (2) lower-order intertidal creeks have a minor role related to the local establishment of such preferential surface flow pathways.

This finding on the role of intertidal creeks, hydraulic connectivity, and flood/ebb dominance has possible implications for salt marsh restoration and morphodynamics. For instance, it is known that stronger peak flood velocity combined with a short flood duration favors landward movement of sediment onto the marsh, thereby promoting accretion in the marsh interior (Aubrey, 1986; Christiansen et al., 2000; Leonard et al., 1995; Stevenson et al., 1988; Van de Kreeke & Robaczewska, 1993; Van Maren & Winterwerp, 2013). It follows that flood dominance can be attributed to young salt marsh basins with low intertidal relief relative to the tidal prism (Boon & Byrne, 1981; Friedrichs & Aubrey, 1988), and ebb dominance with "old" or highly incised marsh (high *Dd*). In the case of Groves Creek, we speculate that the switch to flood dominance for 1–4 is analogous to flow conditions during earlier development of the Groves Creek landscape when *Dd* was lower and hydraulic connectivity was less developed. Also, the reference represents a mature marsh with high *Dd* and well-developed creek networks (Bartholdy et al., 2018; Boon & Byrne, 1981) that increase the potential for short-circuiting. As for the significance of this work toward salt marsh restoration, this work shows that low-order creeks have a minor role in overall high tide circulation and, therefore, replication or restoration of such creeks is not critical to replication of flow dynamics.

Much more information on the role of intertidal creeks in overmarsh circulation can be gleaned through assessing tracer dispersal. In particular, the reference produces greater tracer exchange via Hannah's Creek relative to Groves Creek, and the same is true for 1–2, in addition to slightly enhanced dispersal. However, at 1–4 the tracer is less disperse, and Groves Creek assumes a dominant role in tracer exchange (see data in Table S7). Hence, lower-order creeks have minimal impact on tracer simulations, while removing higher-order creeks limits tracer dispersal and alters pathways for tracer exchange between the marsh interior and the larger subtidal system. This finding contrasts with Blanton et al. (2010), who speculated that circulation of Groves Creek is highly sensitive to small-scale "capillary" creeks less than ~1 m in width and depth. Whereas they attributed their limited tracer dispersal and retention to the absence of small-scale creeks in their flow domain, we speculate that this condition arose because the short-circuiting conduits were not adequately resolved in the bathymetry of their simulations. The latter finding is also particularly relevant to establishing salt marsh restoration guidelines and goals.

The tracer retention estimates highlight a systematic, albeit subtle, decrease in residence time as *Dd* is reduced. With 1–2 residence time decreases by 5%, and with 1–4 it is 14% shorter. From a geomorphic perspective, we propose that a low *Dd* means that the number of topographic pathways for tracer particles decreases and this preferentially routes particles toward the hydraulic connections between the marsh interior and the subtidal system faster, thereby reducing residence time. In the case of 1–4, however, tracer dispersal is limited to the marsh interior, and within close proximity of the Groves Creek system, shortening the path distance required for particles to re-enter the subtidal system on ebb, and this also reduces residence time. This finding has potential implications for assessing contaminant dispersal in salt marshes, and with material exchange between the marsh and the subtidal system. High *Dd* and associated residence time will promote wider and prolonged exposure of the marsh surface to suspended materials and could positively impact eco-geomorphic feedbacks that promote accretion associated with sea level rise (Day et al., 1998; French & Spencer, 1993; Leonard, 1997; Kirwan & Megonigal, 2013; Reed, 1995; Wolaver et al., 1988). However, a 4-m-tall bluff encloses the basin along its lowest elevation, and this will inhibit the creation of new marsh, or migration, at the landward margin, which is also vital to the stability of coastal wetlands under the effects of sea level rise (Cahoon et al., 2006; French, 2006; Kirwan & Megonigal, 2013). Furthermore, reduced sediment supply due to anthropogenic forcing (Syvitski et al., 2005; Tweel & Turner, 2012; Walling, 2006) and climate change (Day et al., 2008) is a major cause for subsidence and salt marsh loss on local (Weston, 2014) and global (Syvitski et al., 2009) scales. Hence, we contend that the Groves Creek marsh may represent a landscape that is "sinking" relative to modern sea level (e.g., Alexander et al., 2017), and, as a consequence, low-order creeks positioned higher up in the tidal framework are no longer of primary importance for flows. Further, with respect to contaminants reaching the salt marsh (e.g., Hamby et al., 1993), our results show that young marshes are less likely to retain contaminant as long as old marshes.

Another important implication of this work relates to marsh restoration. Recent studies have shown that restored marshes generally lack the topographic diversity of their natural counterparts (Brooks et al., 2015) and, more relevant to this study, have significantly lower creek densities than natural marshes (Lawrence et al., 2018). In addition, restored systems have higher sedimentation rates than natural systems (Garbutt et al., 2006; Mazik et al., 2010): a characteristic of flood dominant conditions (Aubrey, 1986;

Christiansen et al., 2000; Stevenson et al., 1988; Leonard et al., 1995; Van de Kreeke & Robaczewska, 1993; Van Maren & Winterwerp, 2013). Collectively, the morphodynamic attributes of restored marshes may be analogous to the 1–4 scenario presented here, with low drainage density and poorly defined hydraulic connectivity between the marsh interior and subtidal system. Moreover, restored marshes are not on a trajectory to become topographically similar to natural marshes with time (Lawrence et al., 2018). Therefore, restoration strategies have considered actively building topographic heterogeneity into the marsh framework to better mirror the morphodynamics of natural sites. Our findings offer this insight for such strategies: constructing the hydraulic connectivity of the landscape, but not necessarily the smallest intertidal creeks, may result in a better representation of natural overmarsh circulation and material exchange. Similarly, Hiatt and Passalacqua (2015) suggested that increased connectivity between channels and marsh interiors could provide engineers a sound avenue for mitigating wetland loss. This work provides an evaluation of how poor representation of subtle topographic features in the bathymetry used to simulate overmarsh circulation might influence assessments or estimates of flows in intertidal landscapes. Hence, our findings offer new insight into the level of topographic detail needed to effectively simulate overmarsh flow, and this has implications for experimental design of future field and numerical studies, on intertidal landscape restoration activities, contaminant retention or circulation, and carbon sequestration. Findings reported here highlight the minor role of small, lower-order creeks in overall circulation and tracer exchange relative to larger, higher-order short-circuiting conduits. Therefore, our work offers this novel insight for numerical studies of overmarsh flow processes: It is of critical importance that the underlying DEM sufficiently resolves the length scale at which hydraulic connectivity and short-circuiting can be established, but not necessarily the smallest intertidal creeks. This level of bathymetric accuracy will provide robust simulation results.

Finally, one might reason that the findings reported here are site specific, largely the outcome of local topographic and hydraulic boundary conditions, and their effects on system-wide circulation. However, the study site is a small part of numerous marshes along the southeastern United States, and the findings reported here are not necessarily unique to Groves Creek. For example, with respect to the idea of short-circuiting, Hiatt and Passalacqua (2015) report from a completely different type of system (open, microtidal, newly formed, perhaps more "regular"-shaped marsh) that hydraulic connectivity between higher-order channels and the marsh interior are the dominant mechanism controlling water circulation and material exchange. Nevertheless, more work is needed to gain a deeper understanding of the influence of basin geometry (shape), variations in vegetation, and local boundary conditions on the relative roles of intertidal creeks and hydraulic connectivity on overmarsh circulation.

6. Conclusions

Sets of numerical simulations of overmarsh flows conducted in response to the successive removal of intertidal creeks show that first- and second-order salt marsh creeks have a minor role in flow processes during marsh inundation, despite a 65% reduction in drainage density. However, smoothing over creeks through Strahler order 4 disrupts connected flow conduits, which facilitate a type of flow "short-circuiting," and this diminished hydraulic connectivity produces a system-wide change from ebb dominance to flood dominance. Creek removal also alters pathways for tracer exchange, and it reduces tracer residence time by 10%. Thus, for the Groves Creek salt marsh the lower-order creeks have a minor role in overmarsh circulation, while higher-order creeks that are associated with flow short-circuiting greatly influence overmarsh flow processes. Therefore, in order to effectively simulate overmarsh flow conditions, the underlying DEM should have a resolution sufficient to characterize the connecting conduits. In other words, the length scale of the underlying DEM should be of sufficient resolution to identify the connecting conduits, but not necessarily the smallest intertidal creeks. For this study, the length scale is about 10 m or the average mouth widths of higher-order creeks.

Acknowledgments
We gratefully acknowledge the following agencies for supporting this research: U.S. DOE Grant DE-AC09-96SR1850 and PADI Research Foundation Grant 10911. We also thank personnel from the USGS, Deltares and University of Antwerp (Guy Gelfenbaum, Andrew Stevens, Edwin Elias, and Stijn Temmerman) for their technical advice in support of the modeling effort. Critical reviews from three anonymous reviewers are also greatly appreciated. All data reported in this paper are publically available through dx.doi.org/10.4211/hs.caa886183ec94d50a25ea868367c1ee7.

References

Alexander, C. R., Hodgson, J. Y. S., & Brandes, J. A. (2017). Sedimentary processes and products in a mesotidal salt marsh environment: Insights from Groves Creek, GA. *Geo-Marine Letters*, *37*(4), 345–359. https://doi.org/10.1007/s00367-017-0499-1

Allen, J. R. L. (1992). Tidally influenced marshes in the Severn Estuary, Southwest Britain. In J. R. L. Allen, & K. Pye (Eds.), *Saltmarshes: Morphodynamics, conservation and engineering significance* (pp. 123–147). Cambridge, UK: Cambridge University Press.

Allen, J. R. L. (2000). Morphodynamics of Holocene salt marshes: A review sketch from the Atlantic and Southern North Sea coasts of Europe. *Quaternary Science Reviews*, *19*(12), 1155–1231. https://doi.org/10.1016/S0277-3791(99)00034-7

Arneborg, L. (2004). Turnover times for the water above sill level in Gullmar Fjord. *Continental Shelf Research*, *24*(4–5), 443–460. https://doi.org/10.1016/j.csr.2003.12.005

Ashley, G. M., & Zeff, M. L. (1988). Tidal classification for a low-mesotidal salt marsh. *Marine Geology*, *82*(1–2), 17–32. https://doi.org/10.1016/0025-3227(88)90004-7

Aubrey, D. G. (1986). Hydrodynamic controls on sediment transport in well-mixed bays and estuaries. In *Physics of shallow estuaries and bays* (pp. 245–258). New York: Springer-Verlag. https://doi.org/10.1029/LN016p0245

Austin, T. P., Short, A. D., Hughes, M. G., Vila-Concejo, A., & Ranasinghe, R. (2009). Tidal hydrodynamics of a micro-tidal, wave dominanted flood-tide delta: Port Stephens, Austrailia. *Journal of Coastal Research*, 693–697.

Bartholdy, J., Brivio, L., Bartholdy, A., Kim, D., & Fruergaard, M. (2018). The Skallingen spit, Denmark: Birth of a back-barrier saltmarsh. *Geo-Marine Letters*, *38*(2), 153–166. https://doi.org/10.1007/s00367-017-0523-5

Bent, E. L., Postma, A., & Stive, R. (1991). Hydrodynamic and dispersion modelling of Swansea Bay. *Environmental Hydraulics*, *1*, 865–870.

Blanton, J. O., Garrett, A. J., Bollinger, J. S., Hayes, D. W., Koffman, L. D., Amft, J., & Morre, T. (2010). Transport and retention of a conservative tracer in an isolated creek-marsh system. *Estuarine, Coastal and Shelf Science*, *87*(2), 333–345. https://doi.org/10.1016/j.ecss.2010.01.010

Boon, I. I. I. J. D., & Byrne, R. J. (1981). On basin hypsometry and the morphodynamic response of coastal inlet systems. *Marine Geology*, *40*(1–2), 27–48. https://doi.org/10.1016/0025-3227(81)90041-4

Brooks, K. L., Mossman, H. L., Chitty, J. L., & Grant, A. (2015). Limited vegetation development on a created salt marsh associated with over-consolidated sediments and lack of topographic diversity. *Estuaries and Coasts*, *38*(1), 325–336. https://doi.org/10.1007/s12237-014-9824-3

Brown, J. M., & Davies, A. G. (2010). Flood/ebb tidal asymmetry in a shallow sandy estuary and the impact on net sand transport. *Geomorphology*, *114*(3), 431–439. https://doi.org/10.1016/j.geomorph.2009.08.006

Cahoon, D. R., Hensel, P. F., Spencer, T., Reed, D. J., McKee, K. L., & Saintilan, N. (2006). Coastal wetland vulnerability to relative sea level rise: Wetland elevation trends and process controls. In *Wetlands and natural resource management* (pp. 271–292). Berlin, Heidelberg: Springer.

Camacho, R. A., Martin, J. L., Diaz-Ramirez, J., McAnnaly, W., Rodriguez, H., Suscy, P., & Zhang, S. (2014). Uncertainty analysis of estuarine hydrodynamic models: An evaluation of input data uncertainty in the Weeks Bay estuary, Alabama. *Applied Ocean research*, *47*, 138–153. https://doi.org/10.1016/j.apor.2014.04.004

Cavalcante, G. H. (2015). Tidal asymmetry. In M. J. Keenish (Ed.), *Encyclopedia of estuaries*. (Chap. 183). Dordrecht. Springer Science & Buisness Media. https://doi.org/10.1007/978-94-017-8801-4

Cea, L., & French, J. R. (2012). Bathymetric error estimation for the calibration and validation of estuarine hydrodynamic models. *Estuarine, Coastal and Shelf Science*, *100*, 124–132. https://doi.org/10.1016/j.ecss.2012.01.004

Chen, S., Torres, R., & Goni, M. (2016). The role of salt marsh structure in the distribution of surface sedimentary organic matter. *Estuaries and Coasts*, *39*(1), 108–122. https://doi.org/10.1007/s12237-015-9957-z

Christiansen, T., Wiberg, P. L., & Milligan, T. G. (2000). Flow and sediment transport on a tidal salt marsh. *Estuarine, Coastal and Shelf Science*, *50*(3), 315–331. https://doi.org/10.1006/ecss.2000.0548

Csanady, G. T. (Ed) (1973). *Turbulent diffusion in the environment (No. 3)*. Dordrecht, Holland, Springer Science. https://doi.org/10.1007/978-94-010-2527-0

Dankers, N., Binsbergen, M., Zegers, K., Laane, R., & van der Loeff, M. R. (1984). Transportation of water, particulate and dissolved organic and inorganic matter between a salt marsh and the Ems-Dollard estuary, the Netherlands. *Estuarine, Coastal and Shelf Science*, *19*(2), 143–165. https://doi.org/10.1016/0272-7714(84)90061-1

Day, J. W., Christian, R. R., Boesch, D. M., Yanez-Arncibia, A., Morris, J., Twilley, R. R., et al. (2008). Consequences of climate change on the ecogeomorphology of coastal wetlands. *Estuaries and Coasts*, *31*(3), 477–491. https://doi.org/10.1007/s12237-008-9047-6

Day, J. W., Rismondo, A., Scarton, F., Are, D., & Cecconi, G. (1998). Relative Sea level rise and Venice lagoon wetlands. *Journal of Coastal Conservation*, *4*(1), 27–34. https://doi.org/10.1007/BF02806486

Delft3D-FLOW UM (2013). *Delft3D-FLOW user manual* (3.14 ed.). Delft, Netherlands: Deltares.

Dronkers, J. (1986). Tidal asymmetry and estuarine morphology. *Netherlands Journal of Sea Research*, *20*(2–3), 117–131. https://doi.org/10.1016/0077-7579(86)90036-0

Esselink, P., Dijkema, K. S., Reents, S., & Hageman, G. (1998). Vertical accretion and profile changes in abandoned man-made tidal marshes in the Dollard estuary, the Netherlands. *Journal of Coastal Research*, 570–582.

Falcao, A. P., Mazzolari, A., Goncalves, A. B., Araujo, M. A. V., & Trigo-Teixeira, A. (2013). Influence of elevation modelling on hydrodynamic simulations of a tidally-dominated estuary. *Journal of Hydrology*, *497*, 152–164. https://doi.org/10.1016/j.jhydrol.2013.05.045

French, J. R. (2006). Tidal marsh sedimentation and resilience to environmental change: Exploratory modelling of tidal, sea-level and sediment supply forcing in predominantly allochthonous systems. *Marine Geology*, *235*(1–4), 119–136. https://doi.org/10.1016/j.margeo.2006.10.009

French, J. R., & Spencer, T. (1993). Dynamics of sedimentation in a tide-dominated back barrier salt marsh, Norfolk, UK. *Marine Geology*, *110*(3–4), 315–331. https://doi.org/10.1016/0025-3227(93)90091-9

French, J. R., & Stoddart, D. R. (1993). Hydrodynamics of salt marsh creek systems: Implications for marsh morphological development and material exchange. *Earth Surface Processes and Landforms*, *17*(3), 232–252.

Friedrichs, C. T., Armbrust, B. A., & De Swart, H. E. (1990). Hydrodynamics and equilibrium sediment dynamics of shallow, funnel-shaped tidal estuaries. In *Physics of estuaries and coastal seas, Rotterndam* (pp. 315–545). The Netherlands: Balkema Press.

Friedrichs, C. T., & Aubrey, D. G. (1988). Non-linear tidal distortion in shallow well-mixed estuaries: A synthesis. *Estuarine, Coastal and Shelf Science*, *27*(5), 521–545. https://doi.org/10.1016/0272-7714(88)90082-0

Friedrichs, C. T., & Perry, J. E. (2001). Tidal salt marsh morphodynamics: A synthesis. *Journal of Coastal Research*, 7–37.

Garbutt, R. A., Reading, C. J., Wolters, M., Gray, A. J., & Rothery, P. (2006). Monitoring the development of intertidal habitats on former agricultural land after the managed realignment of coastal defenses at Tollesbury, Essex, UK. *Marine Pollution Bulletin*, *53*(1–4), 155–164. https://doi.org/10.1016/j.marpolbul.2005.09.015

Gillibrand, P. A. (2001). Calculating exchange times in a Scottish fjord using a two-dimensional, laterally-integrated numerical model. *Estuarine, Coastal and Shelf Science*, *53*(4), 437–449. https://doi.org/10.1006/ecss.199.0624

Hamby, D. M., Addis, R. P., Beals, D. M., Boni, A. L., & Cadieux, J. R. (1993). Environmental monitoring and dose assessment following the December 1991 K-Reactor aqueous tritium release. *Health Physics*, *65*(1), 25–32. https://doi.org/10.1097/00004032-199307000-00004

Hiatt, M., & Passalacqua, P. (2015). Hydraulic connectivity in river deltas: The first-order importance of channel-island exchange. *Water Resources Research*, *51*, 2264–2282. https://doi.org/10.1002/2014WR016149

Jewell, S. A., Walker, D. J., & Fortunato, A. B. (2012). Tidal asymmetry in a coastal lagoon subject to a mixed tidal regime. *Geomorphology*, *138*(1), 171–180. https://doi.org/10.1016/j.geomorph.2011.08.032
Kirwan, M. L., & Megonigal, J. P. (2013). Tidal wetland stability in the face of human impacts and sea-level rise. *Nature*, *504*(7478), 53–60. https://doi.org/10.1038/nature12856
Lawrence, P. J., Smith, G. R., Sullivan, M. J., & Mossman, H. (2018). Restored saltmarshes lack the topographic diversity found in natural habitat. *Ecological Engineering*, *115*, 58–66. https://doi.org/10.1016/j.ecoleng.2018.02.007
Leonard, L. A. (1997). Controls of sediment transport and deposition in an incised mainland marsh basin, southeastern North Carolina. *Wetlands*, *17*(2), 263–274. https://doi.org/10.1007/BF03161414
Leonard, L. A., Hine, A. C., Stumpf, R. P., & Wright, E. E. (1995). Sediment transport processes in a west-central Florida open marine marsh tidal creek; the role of tides and extra-tropical storms. *Estuarine, Coastal and Shelf Science*, *41*(2), 225–248. https://doi.org/10.1006/ecss.1995.0063
Leopold, L. B., Collins, J. N., & Collins, L. M. (1993). Hydrology of some tidal channels in estuarine marshlands near San Francisco. *Catena*, *20*(5), 469–493. https://doi.org/10.1016/0341-8162(93)90043-O
Lesser, G.R. (2000). Computation of three-dimensional suspended sediment transport within the Delft3D-FLOW module, (M.S. thesis), UNESCO-IHE Institute for Water Education, Delft, The Netherlands.
Lincoln, J. M., & Fitzgerald, D. M. (1988). Tidal distortions and flood dominance at five small tidal inlets in southern Maine. *Marine Geology*, *82*(3–4), 133–148. https://doi.org/10.1016/0025-3227(88)90137-5
Maleika, W. (2015). The influence of the grid resolution on accuracy of the digital terrain model used in seabed modeling. *Marine Geophysical Research*, *36*(1), 35–44. https://doi.org/10.1007/s11001-014-9236-6
Marani, M., Belluco, E., D'Alpaos, A., Defina, A., Lanzoni, S., & Rinaldo, A. (2003). On the drainage density of tidal networks. *Water Resources Research*, *39*(2), 1040. https://doi.org/10.1029/2001WR001051
Mazik, K., Musk, W., Dawes, O., Solyanko, K., Brown, S., Mander, L., & Elliott, M. (2010). Managed realignment as compensation for the loss of intertidal mudflat: A short term solution to a long term problem? *Estuarine, Coastal and Shelf Science*, *90*(1), 11–20. https://doi.org/10.1016/j.ecss.2010.07.009
McKean, J., Tonina, D., Bohn, C., & Wright, C. W. (2014). Effects of bathymetric lidar errors on flow properties predicted with a multi-dimensional hydraulic model. *Journal of Geophysical Research: Earth Surface*, *119*, 644–664. https://doi.org/10.1002/2013JF002897
McLeod, E., Chmura, G. L., Bouillon, S., Salm, R., Bjork, M., Duarte, C. M., et al. (2012). A blueprint for blue carbon: Toward an improved understanding of the role of vegetated coastal habitats in sequestering CO2. *Frontiers in Ecology and the Environment*, *9*(10), 552–560.
Mitchell, A. (2005). *The ESRI guide to GIS analysis* (Vol. 2). Redlands, CA: ESRI Press.
Monsen, N. E., Cloern, J. E., Lucas, L. V., & Monismith, S. G. (2003). A comment on the use of flushing time, residence time, and age as transport time scales. *Limnology and Oceanography*, *47*(5), 1545–1553.
Nepf, H., & Ghisalberti, M. (2008). Flow and transport in channels with submerged vegetation. *Acta Geophysica*, *56*(3), 753–777. https://doi.org/10.2478/s11600-008-0017-y
Novakowski, I. K., Torres, R., Gardner, R. L., & Voulgaris, G. (2004). Geomorphic analysis of tidal creek networks. *Water Resources Research*, *40*, W05401. https://doi.org/10.1029/2003WR002722
Pestrong, R. (1965). The development of drainage patterns on tidal marshes, Stanford University publications, 10(2).
Pethick, J. S. (1980). Velocity surges and asymmetry in tidal channels. *Estuarine and Coastal Marine Science*, *11*(3), 331–345. https://doi.org/10.1016/S0302-3524(80)80087-9
Pethick, J. S. (1984). *An introduction to coastal geomorphology*. London: Edwin Arnold.
Ragotzkie, R. A. (1959). Plankton productivity in estuarine waters of Georgia. *Publications of the Institute of Marine Science University of Texas*, *6*, 146–158.
Raupach, M. R. (1994). Simplified expressions for vegetation roughness length and zero-plane displacement as functions of canopy height and area index. *Boundary-Layer Meteorology*, *71*(1–2), 211–216. https://doi.org/10.1007/BF00709229
Reed, D. J. (1995). The response of coastal marshes to sea-level rise: Survival or submergence. *Earth Surface Processes and Landforms*, *20*(1), 39–48. https://doi.org/10.1002/esp.3290200105
Reed, D. J., Spencer, T., Murray, A. L., French, J. R., & Leonard, L. (1999). Marsh surface sediment deposition and the role of tidal creeks: Implications for created and managed coastal marshes. *Journal of Coastal Conservation*, *5*(1), 81–90. https://doi.org/10.1007/BF02802742
Shahriari, M., & Blumsack, S. (2017). Scaling of wind energy variability over space and time. *Applied Energy*, *195*, 572–585. https://doi.org/10.1016/j.apenery.2017.02.073.
Shaw, J. B., Mohrig, D., & Wagner, R. W. (2016). Flow patterns and morphology of a prograding river delta. *Journal of Geophysical Research: Earth Surface*, *121*, 372–391. https://doi.org/10.1002/2015JF003570
Stevenson, J. C., Ward, L. G., & Kearney, M. S. (1988). Sediment transport and trapping in marsh systems: Implications of tidal flux studies. *Marine Geology*, *80*(1-2), 37–59. https://doi.org/10.1016/0025-3227(88)90071-0
Strahler, A. N. (1952). Hypsometric (area-altitude) analysis of erosional topography. *Geological Society of America Bulletin*, *63*(11), 1117–1142. https://doi.org/10.1130/0016-7606(1952)63[1117:HAAOET]2.0.CO;2
Sullivan, J. C., Torres, R., Garrett, A., Blanton, J., Alexander, C., Robinson, M., et al. (2015). Complexity in salt marsh circulation for a semienclosed basin. *Journal of Geophysical Research: Earth Surface*, *120*, 1973–1989. https://doi.org/10.1002/2014JF003365
Syvitski, J. P., Kettner, A. J., Overeem, I., Hutton, E. W. H., Hannon, M. T., Brakenridge, G. R., et al. (2009). Sinking deltas due to human activities. *Nature Geoscience*, *2*(10), 681–686. https://doi.org/10.1038/ngeo629
Syvitski, J. P., Vorosmarty, C. J., Kettner, A. J., & Green, P. (2005). Impact of humans on the flux of terrestrial sediment to the global coastal ocean. *Science*, *308*(5720), 376–380. https://doi.org/10.1126/science.1109454
Tarboton, D. G., Bras, R. L., & Rodriguea-Iturbe, I. (1991). On the extraction of channel networks from digital elevation data. *Hydrological Processes*, *5*(1), 81–100. https://doi.org/10.1002/hyp.3360050107
Temmerman, S., Bouma, T. J., Govers, G., Wang, Z. B., de Vries, M. B., & Herman, P. M. J. (2005). Impact of vegetation on flow routing and sedimentation patterns: Three dimensional modelling for a tidal marsh. *Journal of Geophysical Research*, *110*, F04019. https://doi.org/10.1029/2005JF000301
Tweel, A. W., & Turner, R. E. (2012). Watershed land use and river engineering drive wetland formation and loss in the Mississippi River birdfoot delta. *Limnology and Oceanography*, *57*(1), 18–28. https://doi.org/10.4319/lo.2012.57.1.0018
Van de Kreeke, J., & Robaczewska, K. (1993). Tide-induced residual transport of coarse sediment: Application to the Ems estuary. *Netherlands Journal of Sea Research*, *31*(3), 209–220. https://doi.org/10.1016/0077-7579(93)90022-K

Van den Boogaard, H., Hoogkamer, M., & Heemink, A. (1993). Parameter identification in particle models. *Stochastic Hydrology and Hydraulics*, *7*(2), 109–130. https://doi.org/10.1007/BF01581420
Van Maren, D. S., & Winterwerp, J. C. (2013). The role of flow asymmetry and mud properties on tidal flat sedimentation. *Continental Shelf Research*, *60*, S71–S84. https://doi.org/10.1016/j.csr.2012.07.010
Vandenbruwaene, W., Bouma, T. J., Meire, P., & Temmerman, S. (2013). Bio-geomorphic effects on tidal channel evolution: impact of vegetation establishment and tidal prism change. *Earth Surface Processes and Landforms*, *38*(2), 122–132.
Vandenbruwaene, W., Meire, P., & Temmerman, S. (2012). Formation and evolution of a tidal channel network within a constructed tidal marsh. *Geomorphology*, *151*, 114–125.
Viero, D. P., & Defina, A. (2016). Water age, exposure time, and local flushing time in semi-enclosed tidal basins with negligible freshwater inflow. *Journal of Marine Systems*, *156*, 16–29. https://doi.org/10.1016/j.jmarsys.2015.11.006
Walling, D. E. (2006). Human impact on land-ocean sediment transfer by the world's rivers. *Geomorphology*, *79*(3-4), 192–216. https://doi.org/10.1016/j.geomorph.2006.06.019
Weston, N. B. (2014). Declining sediments and rising seas: An unfortunate convergence for tidal wetlands. *Estuaries and Coasts*, *37*(1), 1–23. https://doi.org/10.1007/s12237-013-9654-8
Wolaver, T. G., Dame, R. F., Spurrier, J. D., & Miller, A. B. (1988). Sediment exchange between a euhaline salt marsh in South Carolina and the adjacent tidal creek. *Journal of Coastal Research*, *4*(1), 17–26.